Rapid Communications

Nucleation of stripe domains in thin ferromagnetic films

S. Singh,* H. Gao, and U. Hartmann
Institute of Experimental Physics, Saarland University, D-66041 Saarbrücken, Germany

(Received 22 January 2018; revised manuscript received 12 July 2018; published 27 August 2018)

For almost 50 years, the formation of stripe domains in magnetic thin films has been considered as an abrupt magnetization phase transition driven by an interplay of the intrinsic perpendicular anisotropy and the shape anisotropy. This allows the determination of a critical film thickness for a given value of the intrinsic perpendicular anisotropy. The present experimental and theoretical analysis shows that micromagnetic structures such as domain walls and their junctions considerably soften a magnetic thin film. The consequence is a significant reduction of the critical film thickness with respect to the originally derived value.

DOI: 10.1103/PhysRevB.98.060414

Stripe patterns occur in a variety of disparate systems, including both technical as well as natural and in particular biological ones [1,2]. Among magnetic materials, garnets [3], FeSi sheets [4], shape memory alloys [5,6], various amorphous alloys [7], and a variety of thin films [8–11] show stripe patterns. Magnetic stripe domains (SDs) are formed from both in-plane [4–6] and out-of-plane orientations of the magnetization [3,5,7–11]. An out-of-plane magnetization generates magnetically charged stripes. A component of the magnetization is alternately arranged upwards and downwards to the sample surface [10,12–14].

In the 1960's, thin films of soft magnetic materials, namely, of permalloy (Py), were found to display SDs [13,15–17], despite having a negligible magnetocrystalline anisotropy [18]. These films develop a perpendicular anisotropy from internal stress in conjunction with a nonzero magnetostriction coefficient [19–21] and/or from columnar grains separated by nonmagnetic intergrain boundaries [22,23]. In general, both these sources constitute the intrinsic perpendicular anisotropy constant K_{int} of the film. Due to the interplay of the perpendicular and the in-plane shape anisotropy, there exists a critical thickness of the film beyond which the formation of the SDs takes place [10,12–14,24]. The critical thickness varies with the film deposition conditions because these have an influence on the K_{int} value [19,20,25,26]. Almost 50 years ago, Holz and Kronmüller calculated the domain phase diagram and the critical thickness as a function of K_{int} in their classical and even today frequently cited work [14]. Beyond the critical thickness, Py films show stable and periodically varying out-of-plane components of the magnetization. However, domain walls (DWs) were completely ignored in the original work because an adequate micromagnetic treatment was beyond the possibilities of a numerical approach at that time. As a result, the domains with an in-plane homogeneous magnetization, separated either by Néel or cross-tie walls [12], are abruptly superimposed by SDs all over the film, when increasing the thickness beyond the critical value [10,12,14].

In the past few decades, magnetic thin films showing SDs were proposed for Bloch-line memories [27], magneto-optical displays [28], and tunable microwave applications due to the presence of a rotatable anisotropy [29]. Recently, SDs have generated new interests for spin-wave propagation in magnonic devices [30] and a nanoscale control of superconductivity in hybrid ferromagnet-superconductor memories [31,32]. Today, much research is focused on the analysis and manipulation of micromagnetic entities, such as DWs [33–36], vortices [35,37,38], and skyrmions [39,40], to enable various new applications of magnetic thin films [33,36,38,40,41]. Consequently, an increasing interest in the fine structures of DWs separating SDs [42,43], in the static and dynamic analysis of SDs in submicron geometries [44–48], and as well in the local tailoring of perpendicular anisotropies [49,50] in various thin films, has developed. In this context, the influence of reduced lateral dimensions on the orientation of an effective anisotropy in SDs was explored [44,45,51]. Also, recently it was shown that skyrmions can be created by passing SDs through geometrical constrictions [52] as well as by a local tuning of the perpendicular anisotropy of thin films [50]. In submicron disks, a range of domain configurations akin to skyrmions besides vortices was observed depending upon the perpendicular anisotropy [46,53]. The fine structure of vortices and skyrmions, which determines their magnetic properties, can be controlled through the perpendicular anisotropy of the film [46,47,50,54]. Recent research further shows that the perpendicular anisotropy of a thin film modifies the DW fine structures in a subtle way [55].

In this Rapid Communication, we focus on the role of DWs and their fine structures in the evolution of SDs in order to refine the Holz and Kronmüller domain phase diagram. For this purpose we performed magnetic force microscopy (MFM) investigations on patterned Py thin films of varying thicknesses and compared the experimental results to those of micromagnetic calculations.

The samples consist of $2.3 \times 6.7\ \mu\mathrm{m}^2$ elongated Py rectangles of a thickness of 120, 140, 180, and 240 nm, respectively. They were fabricated by depositing Py ($Ni_{81}Fe_{19}$) by dc magnetron sputtering onto polymer layers previously patterned by electron-beam lithography on top of Si substrates. The

*s.singh@mx.uni-saarland.de

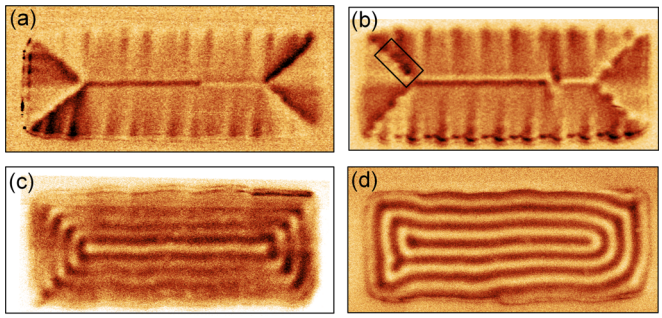

FIG. 1. MFM images of the Landau domain configurations of $2.3 \times 6.7\ \mu m^2$ Py patterns of thickness (a) 120, (b) 140, (c) 180, and (d) 240 nm, respectively. The marked area is shown in more detail in Fig. 4.

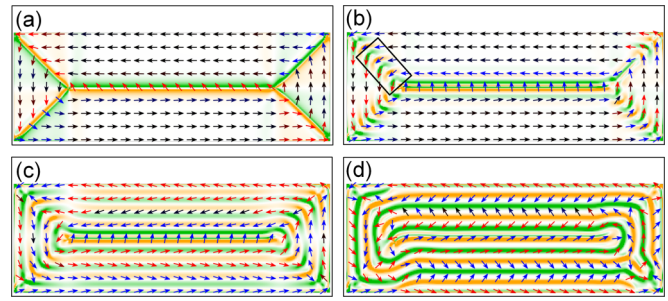

FIG. 2. OOMMF-simulated images of Landau domain configurations in $2.3 \times 6.7\ \mu m^2$ Py patterns of thickness (a) 120 nm with $K_{int} = 0$, (b) 140 nm with $K_{int} = 32.0\ kJ\,m^{-3}$, (c) 180 nm with $K_{int} = 22.5\ kJ\,m^{-3}$, and (d) 240 nm with $K_{int} = 17.0\ kJ\,m^{-3}$, respectively. Each arrow represents an averaged magnetization vector inside 14×14 adjacent cells at the sample surface. Black arrows are in-plane magnetization vectors, whereas blue and red ones are the in-plane projection of magnetization vectors tilted upwards and downwards, respectively. Green and orange areas represent positive and negative charge densities, respectively. The marked area is shown in more detail in Fig. 4.

sputter chamber was evacuated below 1.0×10^{-5} mbar prior to deposition. As the magnetic properties of the films vary with the deposition conditions [19,20,25,26], a constant argon pressure of 2.0×10^{-3} mbar and a sputter rate of 18 nm/min were maintained during the deposition of all samples. The deposition time was varied to achieve different sample thicknesses. Subsequently, the lift-off process was carried out in acetone and the samples were finally cleaned in de-ionized water. The magnetic domain configurations of the samples were analyzed utilizing Olympus AC240TS cantilevers coated with a 30-nm-thick CoCr layer in a Veeco multimode MFM.

Figure 1 shows modifications of the Landau domain configuration at varying sample thicknesses. In Fig. 1(a), for a 120-nm-thick sample, the 90° DWs of the Landau configuration show a continuous bipolar contrast and the 180° DW a unipolar one with a reversal along the wall axis. All these DWs are two-dimensional asymmetric DWs (ADWs) with out-of-plane components (Bloch part) of the magnetization in the interior and in-plane components (Néel caps, NCs) of the magnetization at the surfaces to reduce stray-field energy [12,56,57]. ADWs are further classified into asymmetric Bloch walls (ABWs) and asymmetric Néel walls (ANWs). The ABWs are formed at a wall angle close to 180°. The magnetizations of the upper and lower NCs are oppositely oriented [12]. For a wall angle close to 90°, ANWs are formed. The magnetizations of the upper and lower NCs are rotated by 90° with respect to each other [12]. The reversal in the MFM contrast of the 180° DW in Fig. 1(a) is due to a transition between clockwise and counterclockwise orientations of the Bloch parts [57,58]. Furthermore, the domains show a faint spike-shaped contrast at the edges. This contrast is due to magnetic charges evolving at the imperfect edges of the sample. However, for the 140-nm-thick sample, a periodically changing contrast along the 90° ANWs and a bipolar contrast along the 180° ABW are observed, as shown in Fig. 1(b). These DW modifications for the thinner sample are clearly not related to the perturbed magnetization close to the nonuniform edges of the sample. Upon increasing the sample thickness to 180 nm, the periodic pattern of the 90° ANWs and the bipolar contrast of the 180° ABW are further extended inside the domains. At this thickness, a faint stripe contrast is observed inside the domains as shown in Fig. 1(c). For 240-nm thickness, clear SDs are observed all over the sample, as shown in Fig. 1(d).

For micromagnetic calculations, the object oriented micromagnetic framework (OOMMF) [59] with a cubic cell of 20-nm edge length was used. We assumed a saturation magnetization of $M_s = 860 \times 10^3\ A\,m^{-1}$, an exchange constant of $A = 13 \times 10^{-12}\ J\,m^{-1}$, and a gyromagnetic ratio of $\gamma = 2.21 \times 10^5\ m(A\,s)^{-1}$. To perform the static simulations, a damping parameter of $\alpha = 0.5$ was applied. The convergence criterion $|M \times H|/M_s^2 \leqslant 1 \times 10^{-5}$ as a torque minimization condition was employed in the calculations. In order to mimic the Landau domain configuration obtained in the experimental results, the simulations were started from this configuration as the ground state. This ground state was then allowed to relax for different thicknesses at different values of K_{int} in order to match the experimental results most precisely. K_{int} was increased from zero with a step size of $0.5\ kJ\,m^{-3}$ for each thickness. The shape anisotropy of the film was not included into the perpendicular anisotropy constant K_{int}.

Figure 2 shows the respective theoretical results. Almost perfect matching is achieved in all cases by choosing appropriate values for K_{int}. Figure 3 shows the corresponding cross-sectional images taken from the middle of the samples. In Figs. 2(a) and 3(a) no perpendicular anisotropy had to be assumed to match the experimental results. The spikes observed in Figs. 1(a) and 1(b) are absent in the calculated images because ideally smooth edges of the sample were assumed. The absence of the transition in the 180° wall from Figs. 1(a) and 1(b) is simply due to the initial assumption of a nonsubdivided wall. For the 140-nm-thick sample, no periodic contrast along the 90° DWs and no bipolar contrast along the 180° DW are observed in the simulated images upon assuming a vanishing perpendicular anisotropy. However, a nearly perfect match with the experimental results is obtained upon assuming a perpendicular anisotropy of $K_{int} = 32.0\ kJ\,m^{-3}$. This is shown in Fig. 2(b). Furthermore, though the finite K_{int} value modifies the magnetization inside the DWs, the magnetization inside the domains is still completely in plane. This is in particular evident from Fig. 3(b). A satisfying match of the MFM image from

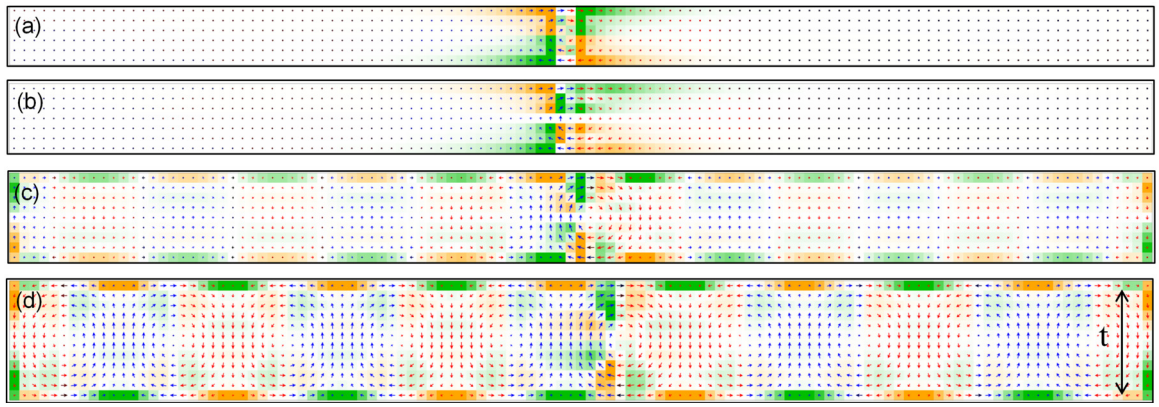

FIG. 3. OOMMF-simulated cross-sectional images of Py films of a thickness t of (a) 120 nm with $K_{\text{int}} = 0$, (b) 140 nm with $K_{\text{int}} = 32.0$ kJ m^{-3}, (c) 180 nm with $K_{\text{int}} = 22.5$ kJ m^{-3}, and (d) 240 nm with $K_{\text{int}} = 17.0$ kJ m^{-3}, respectively. Red and blue arrows represent the out-of-plane projection of the magnetization inside a single cell. Green and orange areas represent positive and negative charge densities, respectively.

Fig. 1(c) was obtained by assuming $K_{\text{int}} = 22.5$ kJ m^{-3}. This is shown in Fig. 2(c). The corresponding cross-sectional image in Fig. 3(c) clearly indicates the slightly upwards and downwards periodic tilting of the magnetization inside the domains. The tilted magnetization in turn produces charges on the sample surfaces. In Fig. 2(d), the SDs inside the 240-nm-thick Py sample were reproduced by assuming $K_{\text{int}} = 17.0$ kJ m^{-3}. The corresponding cross-sectional image is shown in Fig. 3(d). An increased tilting of the magnetization inside the domains is clearly visible.

In Fig. 4, details in terms of charged segments from modified 90° ANW are visible. By comparing both images in detail, it becomes clear that the periodically varying magnetic charges along the walls are formed because of periodically upwards and downwards pointing DW segments. Since no changes are yet induced within the domains, the DWs are clearly magnetically softest.

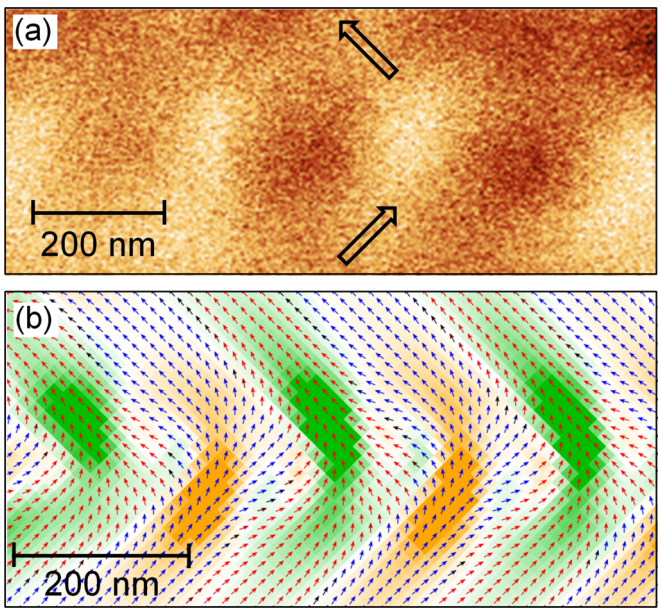

FIG. 4. Modified 90° ANW of the 140-nm-thick sample. (a) Enlarged MFM image of the area marked in Fig. 1(b). Arrows represent the direction of magnetization. (b) Simulated data corresponding to Fig. 2(b). Each arrow represents an in-plane magnetization vector inside a single cell. Blue and red arrows represent the in-plane projection of magnetization vectors tilted upwards and downwards, respectively. Green and orange areas represent positive and negative charge densities, respectively.

In order to explore the three-dimensional modifications of the wall fine structures induced by the perpendicular anisotropy in more detail, magnetization vector fields were modeled for a 140-nm-thick sample for both $K_{\text{int}} = 0$ and $K_{\text{int}} = 32.0$ kJ m^{-3}. The resulting configurations of the DWs are compared in Fig. 5. From Figs. 5(a) and 5(b), it is observed that the perpendicular anisotropy increases the magnitude of the out-of-plane tilting in the preexisting Bloch part of the DWs. This in turn enhances the divergences of the magnetization at the intersection of the ANW with the sample surfaces and hence increases the charge densities right at the surfaces. Furthermore, from Figs. 5(c) and 5(d), it is clear that in order to reduce the stray field energy, the ANW splits into periodically upwards and downwards magnetized segments in its interior. The relative orientation of the upper and lower NCs still remains at 90°. Figures 5(e) and 5(f) schematically illustrate the respective ANW configurations.

The 180° ABWs in all images of Figs. 1 and 2 do not show periodically varying charges at the sample surfaces. However, the MFM contrast changes from unipolar to bipolar as seen in Figs. 1(a) and 1(b). Subsequently, a faint stripe contrast appears along the ABW with further increasing sample thickness. According to Fig. 3, the 180° ABW involves a vortex structure in its cross section. This vortex picks up a big part of the increase in the magnetization divergence and hence prevents the splitting of the out-of-plane components in the interior of the ABWs. However, with the increase of sample thickness, the periodically upwards and downwards magnetized segments are spreading parallel to the 180° ABW on both sides, as seen in Fig. 3(b). The expanding segments cross the 90° ANWs and are ultimately extended all over the sample with further increasing thickness. This finally constitutes a complete SD pattern as predicted by the Holz-Kronmüller nucleation model.

In Fig. 6, the thickness dependence of K_{int} as obtained from a comparison of experimental and theoretical data is shown. Furthermore, the thickness dependence of a computationally

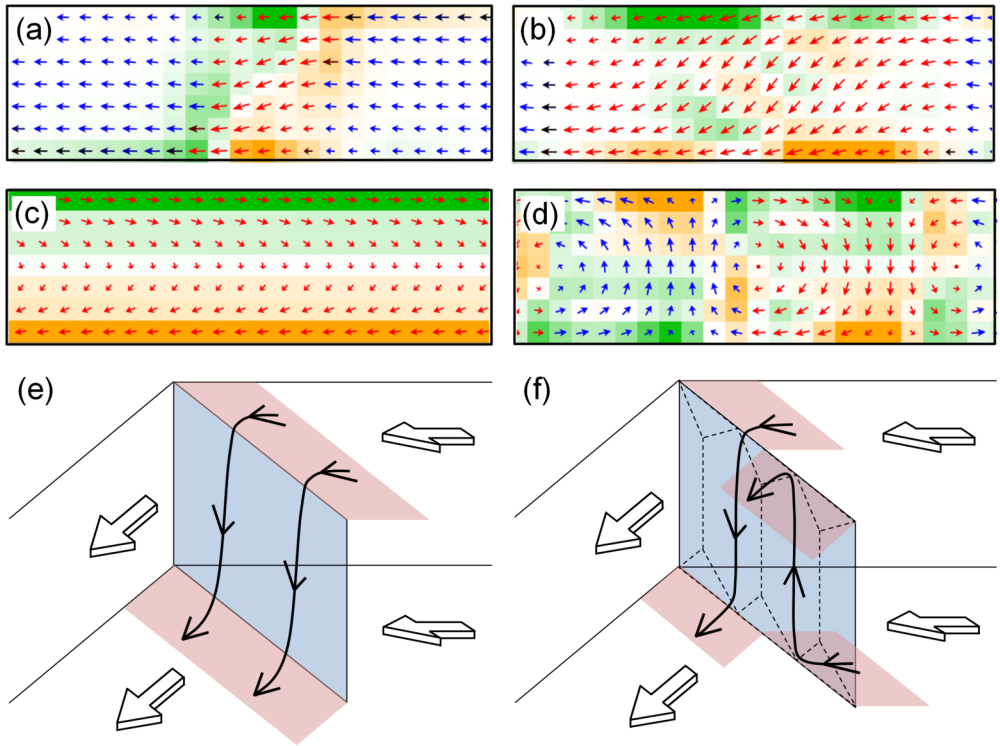

FIG. 5. A 90° ANW with $K_{\text{int}} = 0$ in (a), (c) and (e) is compared with a 90° ANW with $K_{\text{int}} = 32.0\,\text{kJ m}^{-3}$ in (b), (d), and (f) for a 140-nm-thick sample, respectively. (a)–(d) show simulated images of the 90° ANW and each arrow in the simulated images represents an out-of-plane projection of the magnetization vector inside a single cell. (a) and (b) show cross-sectional images of the DW. (c) and (d) show views along the wall axis. (e) and (f) schematically show the 90° ANW. The bold arrows represent the magnetization inside the domains, whereas the magnetization inside the DW is represented by curved lines. The blue shaded areas represent those parts of the ANW which have out-of-plane magnetization components (i.e., Bloch parts) and the red shaded areas represent NCs with in-plane components at the surfaces.

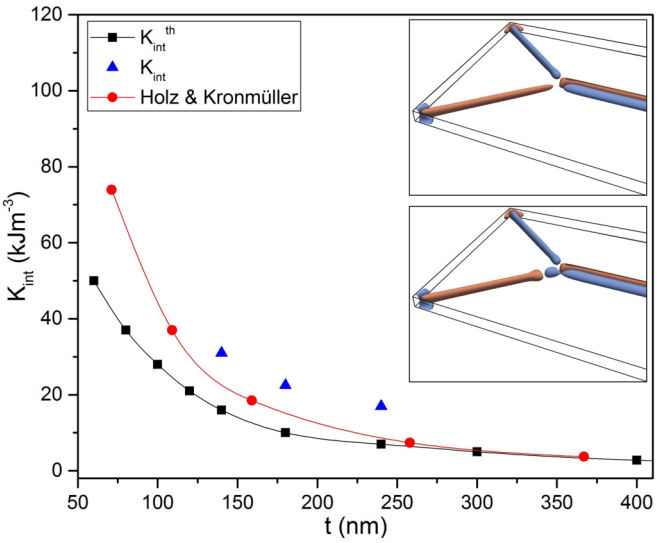

FIG. 6. Thickness dependence of K_{int} (blue triangles) and $K_{\text{int}}^{\text{th}}$ (black squares) for Py thin films. Data from Holz and Kronmüller [14] are shown as red dots. The area below the $K_{\text{int}}^{\text{th}}$ data points represents the thickness regime in which the perpendicular anisotropy does not induce any magnetization reversal. The upper and lower insets show the magnetization isosurfaces at the wall junctions for an out-of-plane component of $M_z = \pm 0.25 M_s$ in the 140-nm-thick sample for $K_{\text{int}} = 15\,\text{kJ m}^{-3}$ and $K_{\text{int}} = 16\,\text{kJ m}^{-3}$, respectively. Blue and red represent upwards and downwards oriented magnetizations, respectively.

obtained threshold anisotropy $K_{\text{int}}^{\text{th}}$ is shown as well. When K_{int} exceeds this value, the first magnetization reversal processes along the DWs lead to increasing out-of-plane components. For a 140-nm-thick sample, an increase of K_{int} up to $15\,\text{kJ m}^{-3}$ does not cause any observable magnetization reversal as seen in the upper inset of Fig. 6. However, such a reversal is observed for the slightly bigger value of $K_{\text{int}} = 16\,\text{kJ m}^{-3}$ shown in the lower inset of Fig. 6 (see the Supplemental Material [60]). Figure 6 also shows the classical data calculated by Holz and Kronmüller [14]. Comparing these data to our results, it can be concluded that the DWs magnetically soften the sample and permit the evolution of premature SDs at an anisotropy well below the one needed for a sudden nucleation of complete SDs. The experimentally observed K_{int} values are well above the threshold values.

A decrease of K_{int} with increasing film thickness as observed here was also reported in Ref. [61]. A plausible explanation for this behavior is that stresses due to the lattice mismatch at the Py-substrate interface decrease with increasing distance to the interface [61,62]. Therefore, the effective value of K_{int} decreases with increasing film thickness. However, with increasing thickness the shape anisotropy decreases as well (see the Supplemental Material [60]). Therefore, above a certain critical thickness, SDs develop in spite of a decreasing intrinsic anisotropy K_{int}.

To conclude, we have refined the almost 50-year-old domain phase diagram by Holz and Kronmüller [14] by showing that the formation of stripe domains is an evolutionary and

continuous process, which starts well below the critical thickness expected for the formation of the stripe phase from classical theory. The stripe domains evolve from the domain walls and, in particular, wall junctions which locally soften the film. Particularly interesting is that these softening sites shift the development of full stripe domains to film thicknesses which are for a given perpendicular anisotropy even above those values predicted by Holz and Kronmüller. We have shown that the initial changes of the magnetization due to a perpendicular anisotropy start at magnetic inhomogeneities, i.e., domain walls and wall junctions. Structural imperfections and crystalline defects of magnetic films also result in magnetic inhomogeneities [63]. Thus, the presented results are of some general relevance and conclusions are not limited to configurations involving domain walls only. In general, the tailoring of fine structures of micromagnetic entities in the context of spintronics is of great importance today [64,65]. This definitely implies manifold implications of the presented results for applications of magnetic thin films in present and future technologies.

[1] C. Bowman and A. C. Newell, Rev. Mod. Phys. **70**, 289 (1998).
[2] D. Andelman and R. E. Rosensweig, J. Phys. Chem. B **113**, 3785 (2009).
[3] M. Seul and D. Andelman, Science **267**, 476 (1995).
[4] O. Perevertov, J. Thielsch, and R. Schäfer, J. Magn. Magn. Mater. **385**, 358 (2015).
[5] Y.-W. Lai, R. Schäfer, L. Schultz, and J. McCord, Appl. Phys. Lett. **96**, 022507 (2010).
[6] M. Wuttig, J. Li, and C. Craciunescu, Scr. Mater. **44**, 2393 (2001).
[7] R. Schäfer, N. Mattern, and G. Herzer, IEEE Trans. Magn. **32**, 4809 (1996).
[8] X. Z. Yu, Y. Onose, N. Kanazawa, J. H. Park, J. H. Han, Y. Matsui, N. Nagaosa, and Y. Tokura, Nature (London) **465**, 901 (2010).
[9] O. Portmann, A. Vaterlaus, and D. Pescia, Nature (London) **422**, 701 (2003).
[10] F. Virot, L. Favre, R. Hayn, and M. D. Kuz'min, J. Phys. D: Appl. Phys. **45**, 405003 (2012).
[11] G. Leaf, H. Kaper, M. Yan, V. Novosad, P. Vavassori, R. E. Camley, and M. Grimsditch, Phys. Rev. Lett. **96**, 017201 (2006).
[12] A. Hubert and R. Schäfer, *Magnetic Domains: The Analysis of Magnetic Microstructures* (Springer, Berlin, 1998).
[13] N. Saito, H. Fujiwara, and Y. Sugita, J. Phys. Soc. Jpn. **19**, 1116 (1964).
[14] A. Holz and H. Kronmüller, Phys. Status Solidi **31**, 787 (1969).
[15] E. E. Huber and D. O. Smith, J. Appl. Phys. **30**, S267 (1959).
[16] R. J. Spain, Appl. Phys. Lett. **3**, 208 (1963).
[17] R. W. DeBlois, J. Appl. Phys. **40**, 1084 (1969).
[18] L. F. Yin, D. H. Wei, N. Lei, L. H. Zhou, C. S. Tian, G. S. Dong, X. F. Jin, L. P. Guo, Q. J. Jia, and R. Q. Wu, Phys. Rev. Lett. **97**, 067203 (2006).
[19] P. Zou, W. Yu, and J. A. Bain, IEEE Trans. Magn. **38**, 3501 (2002).
[20] P. Zou, W. Yu, and J. A. Bain, J. Appl. Phys. **91**, 7830 (2002).
[21] W. Karboul-Trojet, Y. Roussigné, D. Faurie, and S. M. Chérif, Eur. Phys. J. B **85**, 339 (2012).
[22] H. Fujiwara, J. Phys. Soc. Jpn. **20**, 2092 (1965).
[23] N. Amos, R. Fernandez, R. Ikkawi, B. Lee, A. Lavrenov, A. Krichevsky, D. Litvinov, and S. Khizroev, J. Appl. Phys. **103**, 07E732 (2008).
[24] D. S. Lo and M. M. Hanson, J. Appl. Phys. **38**, 1342 (1967).
[25] S. Min, J. A. Bain, and D. W. Greve, J. Appl. Phys. **91**, 6824 (2002).
[26] A. V. Svalov, I. R. Aseguinolaza, A. Garcia-Arribas, I. Orue, J. M. Barandiaran, J. Alonso, M. L. FernÁndez-Gubieda, and G. V. Kurlyandskaya, IEEE Trans. Magn. **46**, 333 (2010).
[27] S. Konishi, IEEE Trans. Magn. **19**, 1838 (1983).
[28] R. J. Spain and H. W. Fuller, J. Appl. Phys. **37**, 953 (1966).
[29] S. Tacchi, S. Fin, G. Carlotti, G. Gubbiotti, M. Madami, M. Barturen, M. Marangolo, M. Eddrief, D. Bisero, A. Rettori, and M. G. Pini, Phys. Rev. B **89**, 024411 (2014).
[30] C. Banerjee, P. Gruszecki, J. W. Klos, O. Hellwig, M. Krawczyk, and A. Barman, Phys. Rev. B **96**, 024421 (2017).
[31] G. Karapetrov, A. Belkin, M. Iavarone, J. Fedor, V. Novosad, M. V. Milošević, and F. M. Peeters, J. Supercond. Novel Magn. **24**, 905 (2011).
[32] B. Baek, W. H. Rippard, S. P. Benz, S. E. Russek, and P. D. Dresselhaus, Nat. Commun. **5**, 1 (2014).
[33] F. Cheynis, A. Masseboeuf, O. Fruchart, N. Rougemaille, J. C. Toussaint, R. Belkhou, P. Bayle-Guillemaud, and A. Marty, Phys. Rev. Lett. **102**, 107201 (2009).
[34] V. D. Nguyen, O. Fruchart, S. Pizzini, J. Vogel, J.-C. Toussaint, and N. Rougemaille, Sci. Rep. **5**, 12417 (2015).
[35] A. Masseboeuf, O. Fruchart, J. C. Toussaint, E. Kritsikis, L. Buda-Prejbeanu, F. Cheynis, P. Bayle-Guillemaud, and A. Marty, Phys. Rev. Lett. **104**, 127204 (2010).
[36] C. Zinoni, A. Vanhaverbeke, P. Eib, G. Salis, and R. Allenspach, Phys. Rev. Lett. **107**, 207204 (2011).
[37] M. Noske, H. Stoll, M. Fähnle, R. Hertel, and G. Schütz, Phys. Rev. B **91**, 014414 (2015).
[38] T. Shinjo, T. Okuno, R. Hassdorf, K. Shigeto, and T. Ono, Science **289**, 930 (2000).
[39] N. Nagaosa and Y. Tokura, Nat. Nanotechnol. **8**, 899 (2013).
[40] A. Fert, N. Reyren, and V. Cros, Nat. Rev. Mater. **2**, 17031 (2017).
[41] R. Hertel, Nat. Nanotechnol. **8**, 318 (2013).
[42] D. Navas, C. Redondo, G. A. Badini Confalonieri, F. Batallan, A. Devishvili, Ó. Iglesias-Freire, A. Asenjo, C. A. Ross, and B. P. Toperverg, Phys. Rev. B **90**, 054425 (2014).
[43] T. Herranen and L. Laurson, Phys. Rev. B **92**, 100405 (2015).
[44] D. Navas, C. Nam, D. Velazquez, and C. A. Ross, Phys. Rev. B **81**, 224439 (2010).
[45] S. H. Lee, F. Q. Zhu, C. L. Chien, and N. Marković, Phys. Rev. B **77**, 132408 (2008).
[46] C. Moutafis, S. Komineas, C. A. F. Vaz, J. A. C. Bland, and P. Eames, Phys. Rev. B **74**, 214406 (2006).
[47] K. Efthimiadis and N. Ntallis, J. Magn. Magn. Mater. **446**, 245 (2018).
[48] H. Niedoba and M. Labrune, J. Magn. Magn. Mater. **321**, 2178 (2009).
[49] A. Hierro-Rodriguez, R. Cid, M. Vélez, G. Rodriguez-Rodriguez, J. I. Martín, L. M. Álvarez-Prado, and J. M. Alameda, Phys. Rev. Lett. **109**, 117202 (2012).
[50] S. Zhang, A. K. Petford-Long, and C. Phatak, Sci. Rep. **6**, 31248 (2016).

[51] O. de Abril, M. d. C. Sánchez, and C. Aroca, J. Appl. Phys. **100**, 063904 (2006).
[52] W. Jiang, P. Upadhyaya, W. Zhang, G. Yu, M. B. Jungfleisch, F. Y. Fradin, J. E. Pearson, Y. Tserkovnyak, K. L. Wang, O. Heinonen, S. G. E. te Velthui, and A. Hoffmann, Science **349**, 283 (2015).
[53] E. R. P. Novais, P. Landeros, A. G. S. Barbosa, M. D. Martins, F. Garcia, and A. P. Guimarães, J. Appl. Phys. **110**, 053917 (2011).
[54] R. Novak, F. Garcia, E. Novais, J. Sinnecker, and A. Guimarães, J. Magn. Magn. Mater. **451**, 749 (2018).
[55] S. Voltan, C. Cirillo, H. J. Snijders, K. Lahabi, A. García-Santiago, J. M. Hernández, C. Attanasio, and J. Aarts, Phys. Rev. B **94**, 094406 (2016).
[56] A. Hubert, Phys. Status Solidi **38**, 699 (1970).
[57] V. V. Zverev, B. N. Filippov, and M. N. Dubovik, Phys. Solid State **56**, 1785 (2014).
[58] H. Asada, H. Kubo, J. Yamasaki, M. Takezawa, and T. Koyanagi, J. Phys.: Conf. Ser. **200**, 042003 (2010).
[59] M. J. Donahue and D. G. Porter, *OOMMF User's Guide, Version 1.0*, NIST Report No. NISTIR 6376 (National Institute of Standards and Technology, Gaithersburg, MD, 1999).
[60] See Supplemental Material at http://link.aps.org/supplemental/10.1103/PhysRevB.98.060414 for details of threshold intrinsic perpendicular anisotropy, interplay of shape and intrinsic perpendicular anisotropy, and the dependence of threshold intrinsic perpendicular anisotropy on saturation magnetization.
[61] J. McCord, B. Erkartal, T. von Hofe, L. Kienle, E. Quandt, O. Roshchupkina, and J. Grenzer, J. Appl. Phys. **113**, 073903 (2013).
[62] G. Janssen, Thin Solid Films **515**, 6654 (2007).
[63] R. M. Vakhitov and E. B. Magadeev, Phys. Met. Metallogr. **115**, 849 (2014).
[64] G. Chen and A. K. Schmid, Adv. Mater. **27**, 5738 (2015).
[65] B. Dupé, M. Hoffmann, C. Paillard, and S. Heinze, Nat. Commun. **5**, 4030 (2014).